Mitochondria-targeted antioxidant MitoQ reduced renal damage caused by ischemia-reperfusion injury in rodent kidneys: longitudinal observations of T_2WI and dynamic contrast-enhanced MRI

Title page

Authors list:

1. Xiaoge Liu Department of Radiology, Tianjin Medical University General Hospital, Tianjin, China
2. Michael P. Murphy Medical Research Council Mitochondrial Biology Unit, Cambridge BioMedical Campus, Cambridge, UK
3. Wei Xing Department of Radiology, Third Affiliated Hospital of Suzhou University, Changzhou, Jiangsu, China
4. Huanhuan Wu Department of Radiology, Tianjin Medical University General Hospital, Tianjin, China
5. Rui Zhang Department of Radiology, Tianjin Medical University General Hospital, Tianjin, China
6. Haoran Sun Department of Radiology, Tianjin Medical University General Hospital, Tianjin, China

Corresponding Author: Haoran Sun. sunhaoran2006@hotmail.com

Address for correspondence: Haoran Sun, Department of Radiology, Tianjin Medical University General Hospital, Tianjin 300052, China

E- Mail: sunhaoran2006@hotmail.com

Abstract

Purpose: To investigate the effect of mitochondria-targeted antioxidant MitoQ in reducing the severity of renal ischemia-reperfusion injury (IRI) in rats using T_2WI and dynamic contrast-enhanced MRI (DCE-MRI).

Methods: IRI was induced by temporarily clamping the left renal artery. Rats were pretreated with MitoQ or saline. MRI examination was performed before and after IRI (days 2, 5, 7 and 14). The T_2-weighted standardized signal intensity (SSI) of the outer stripe of the outer medulla (OSOM) was measured. The unilateral renal clearance rate k_{cl} was derived from DCE-MRI. Histopathology was evaluated after the final MRI examination.

Results: SSI of the OSOM on IRI kidneys with MitoQ were lower than those with saline on day 5 and day 7 (P = 0.004, P < 0.001, respectively). K_{cl} values of IRI kidneys with MitoQ were higher than those with saline at all time points (P = 0.002, P < 0.001, P = 0.001, P < 0.001). Histopathology showed that renal damage was the most predominant on the OSOM of IRI kidneys with saline, which was less obvious with MitoQ (P < 0.001).

Conclusion: These findings demonstrate MitoQ can reduce the severity of renal damage in rodent IRI models using T_2WI and DCE-MRI.

Key Words: kidney; renal function; ischemia-reperfusion injury, IRI; dynamic contrast-enhanced magnetic resonance imaging, DCE-MRI; histopathology

Introduction

Nephron-sparing nephrectomy has been accepted as the standard surgical procedure for the treatment of small renal tumors and in patients with bilateral tumors (1,2). Temporary renal artery occlusion is essential during the operation to prevent intraoperative bleeding and provide a bloodless surgical field (3). Hence, warm ischemia (WI) and subsequently renal ischemia-reperfusion injury (IRI) are inevitable and are a major cause of postoperative renal functional decline (4,5). Kalogeris et al (6) proposed that pharmacological preconditioning could contribute to the activation

of cell survival mechanisms and protection of the kidneys from IRI. The search for novel medical interventions is of great research interest (7). Cell death programs activated by ischemia and reperfusion are related to apoptosis, necrosis, autoimmune responses and enhanced reactive oxygen species (ROS) generation, and there might be a reciprocity between the programs and mitochondrial oxidative damage in the early phases of IRI (8,9). The oxidative stress caused by excessive amount of ROS during IRI could alter mitochondrial oxidative phosphorylation and activate membrane phospholipids proteases, more importantly, oxygen free radicals during reperfusion could result in lipid peroxidation (10). As mitochondrial oxidative damage is central to IRI damage, decreasing mitochondrial oxidative activity during IRI could be a potential therapeutic approach. Since untargeted cellular antioxidants cannot accumulate in mitochondria and they are not protective (11), Murphy et al developed the mitochondria-targeted antioxidant MitoQ. MitoQ is conjugated to a lipophilic cation that can rapidly pass through the mitochondria phospholipid bilayer and accumulate within the mitochondria with the help of the electrochemical gradient (11).

MRI can provide excellent morphologic and functional information for evaluating renal pathophysiology noninvasively in vivo and is suitable for repeated measurements. The differences between T_2 relaxation times for different tissues enable MRI to be used in the evaluation of morphologic changes with high spatial resolution (12). The severity of renal IRI damage varies in different regions. Hueper et al demonstrated that the T_2 values of the outer stripe of the outer medulla (OSOM) could be used to distinguish between severe injury and moderate injury after IRI in mice (13). This capability exists probably because the thick ascending limb of Henle's loop and the S3 segment of the proximal tubule in the OSOM consume far more oxygen than any other parts to achieve sodium balance involving active reabsorption (14). It has been well documented that renal functional parameters obtained from dynamic contrast-enhanced MRI (DCE-MRI) are closely correlated with radionucllde renography parameters(15). Baumann and Rudin proposed that the first-order rate constant k_{cl}, which reflected tracer transportation from the renal cortex to the medulla

in the initial phase of DCE-MRI, might provide a good estimation of the kidney clearance rate (16). Laurent et al (17) further demonstrated that k_{cl} data estimated by DCE-MRI correlated well with GFR values assessed using the inulin clearance assay. In this setting, the left renal artery was clamped and the right kidneys were kept as controls, which made this variable ideal for comparisons to reveal renal morphologic and functional changes bilaterally in living animals. It would be beneficial, both methodologically and ecologically, if the quantitative estimations of T2 signal intensities of the OSOM and k_{cl} values obtained from DCE-MRI before and after IRI could noninvasively reveal the severity of renal damage and be used to evaluate the effect of medical pretreatment in protecting against IRI.

The aim of the study was to investigate the effect of MitoQ in reducing the severity of renal damage caused by IRI in rats based on the longitudinal observations of T_2WI and DCE-MRI with quantitative estimations of unilateral renal dynamic parameters.

Methods

Animal Preparation

This study was approved by the local Animal Care and Use Committee. Twenty male Sprague–Dawley rats (Beijing University Health Science Center) with an average weight of 250 g were used in this experiment. The rats were randomly divided into four groups: Group I (IRI with MitoQ treatment, n = 5), in which the rats were administered with MitoQ (donated by Antipodean Pharmaceuticals Inc.: 2.8 mg/kg in 700 μL 0.9% saline) 15 min prior to the onset of WI via the tail vein at an injection rate of 20 μL/s, then subjected to left renal ischemia for 45 min followed by reperfusion; Group II (IRI with saline treatment, n = 5), which underwent the same procedure as Group I except that the injectant was 700 μL 0.9% saline instead of MitoQ; Group III (normal kidneys with MitoQ treatment, n = 5), in which the rats were administered with MitoQ in the same way as in Group I but without the IRI procedure; and Group IV (normal kidneys with saline treatment, n = 5), in which the rats were administered with saline in the same way as in Group II but without the IRI

procedure.

Ischemia-reperfusion Injury Model

The animals were fasted overnight with free access to water before the operation. They were placed on a homoeothermic pad to maintain body temperature 37±1 °C. Anesthesia was maintained by mask inhalation of isoflurane vaporized at concentrations of 1–2.5% during the operation. The abdominal region was shaved and sterilized. After a midline laparotomy was performed, the left renal artery was isolated and clamped using microvascular clips to reversibly occlude renal blood supply. Complete occlusion was verified by observing the color of the kidney, running from bright red to reddish brown color. A warm ischemia time (WIT) of 45 min was chosen on the basis of previous experience to ensure renal function decline and minimize the mortality of the animals. After the clips were removed when the WIT was up, the kidneys were observed as returning to bright red color, and then the incision was sutured. After the operation, the rats were returned to their cages in a temperature- and humidity-controlled facility with a constant 12 h light/dark cycle.

MRI Examination

MRI scanning was performed before the operation (day 0) and on days 2, 5, 7 and 14 after IRI on a 3T scanner (MR750, GE Healthcare, US) with a 6 cm internal diameter four-channel phase-arrayed animal coil (Magtron, Shenzhen, China). Rats were fasted but free of drinking 2 h before the MRI examination, and anesthesia was maintained by mask inhalation of isoflurane vaporized at concentrations of 1–2.5% during the scanning. Each animal was placed in a supine position, and appropriate compression was applied to the abdominal region to restrict the respiration movement to a minimal extent.

Coronal high-resolution T_2WI (fat-suppressed fast recovery fast spin echo, TR/TE 3106 ms/92 ms; matrix size 352 [frequency] ×352 [phase]; echo train length 22; field of view 6.0×6.0 cm; slice thickness 1.5 mm; slice spacing 0.5 mm; bandwidth

±46.446 kHz, two signal averaged, acquisition time 4 min 13 s) and DCE-MRI (3D liver acceleration volume acquisition, TR/TE 5.3 ms/2.0 ms; flip angle 15 °; bandwidth ±125 kHz; matrix size 160 [frequency]×128 [phase]; freq FOV 13.0 cm; phase FOV 0.80; slice thickness 2 mm; spacing 0 mm) were acquired. For DCE-MRI, a precontrast data set was obtained, after which a bolus injection of 0.04 mmol/kg of diluted Gd-DTPA solution (100–120 μL; Magnivist, Bayer-Schering, Germany, 125 mmol/L) was administered through a catheter in the tail vein at an injection rate of 100 μL/s. DCE-MRI scanning was repeated immediately after the administration of Gd-DTPA. A total of 12 coronal slices were acquired in 3 s, and 20 enhanced phases were continuously obtained in 60 s.

The Relationship between the Signal Intensity and gadolinium-DTPA Concentration

It has been documented that the signal intensity (SI) changes can be converted into longitudinal relaxation rate (R1) changes using a polynomial equation (18), and R1 correlated well with the concentration of Gd-DTPA (19). Besides, there is a linear relationship between SI changes and the increased concentration of Gd-DTPA between 0 mmol/L and 4 mmol/L (20). In the present study, the estimated Gd-DTPA concentration in the renal parenchyma was less than 4 mmol/L because of the low administration dose; therefore, it was feasible to reflect the Gd-DTPA concentration based on the SI.

Image Analysis and k_{cl} Calculation

The SI changes were evaluated on an ADW4.5 GE workstation. The SI of the renal cortex (CO), the outer stripe of the outer medulla (OSOM), the inner stripe of the outer medulla (ISOM) and psoas major on the middle section of bilateral kidneys were inspected on coronal T_2WI. The regions of interest (ROIs) of the OSOM and

homolateral psoas major were delineated (Fig. 1). The renal SI was prone to be affected by the adjacent tissues (intra-abdominal fat or gas in the gastrointestinal tract), while the SI of the psoas major was relatively constant. Therefore, a T2-weighted standardized signal intensity (SSI) was obtained by calculating the ratio of the SI of the OSOM and the homolateral psoas major.

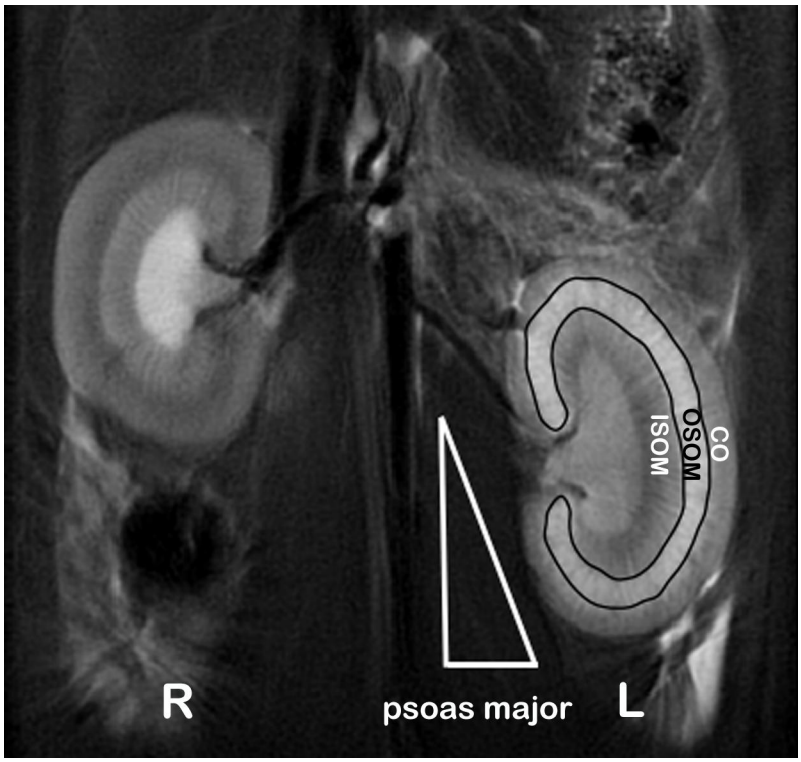

FIG. 1. Example of ROI plotting on coronal fat-suppressed T_2WI after IRI. The renal cortex (CO), the outer stripe of the outer medulla (OSOM) and the inner stripe of the outer medulla (ISOM) are illustrated on the left renal parenchyma. The ROI of the entire OSOM on a central section of the left kidney is delineated by a black line; the left psoas major is delineated by a white triangle.

The DCE-MRI data were analyzed using locally developed software (Northeastern University, Shenyang, China) on a HP workstation. The DCE images were segmented and measured semi-automatically. Firstly, the most optimal phase, when there was a clear corticomedullary demarcation between the CO and the whole medulla (M, including OSOM, ISOM and the inner medulla [IM]) was manually selected among the multiphasic images (Fig. 2a); then, ROIs of the entire CO and M regions were

drawn and copied to the other phases. The ROI of the M was carefully separated from the CO to avoid the partial volume effect (Fig. 2b,c). Secondly, the average SI of the CO and M were calculated, and the absolute SI in each phase was obtained by multiplying the area of the ROI and the slice thickness. The relative SI was determined by subtracting the SI of the precontrast image from the absolute SI. Thirdly, the time-signal intensity curves (TICs) of the CO and the M were plotted and the fitting curve of the SI of the M was determined (Fig. 2d).

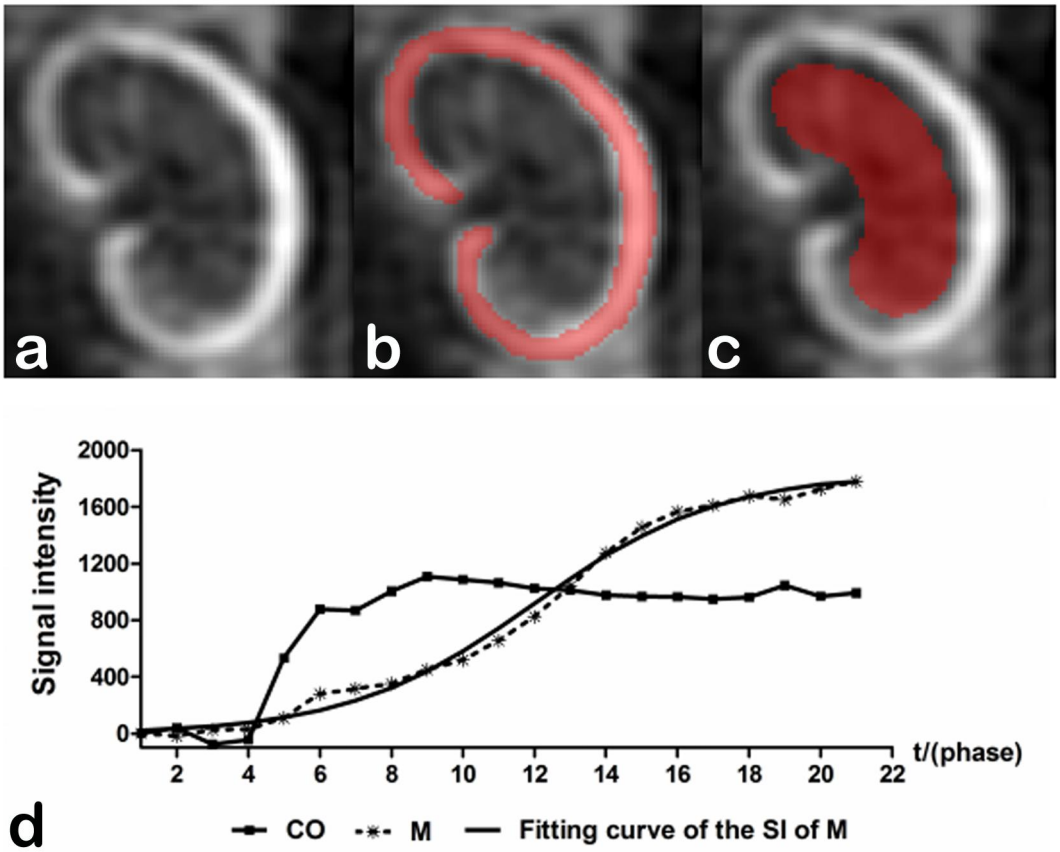

FIG. 2. Example of renal semi-automatic segmentation and ROI setting on DCE-MRI, the time-intensity curves (TICs) of the renal CO and the medulla (M), and the fitting curve of the SI of the M. a. The original contrast-enhanced image of the left kidney. b. The ROI of the CO was recognized automatically and is rendered with a red color. c. The ROI of the M was delineated manually and is shown with a red color; please note that the ROI of the M was carefully separated from the CO to avoid the partial volume effect. d. The TICs of the renal CO, M and the fitting curve of the SI of the M. The TIC of the CO rose radically in the early phases until reaching the platform, while the TIC

of the M kept rising gradually for a long time. The fitting curve of the SI of the M was a smooth curve overlapping the true TIC of the M. Note that the aquasition time in each phase was 3 s.

The clearance rate constant k_{cl} was obtained using the mathematical model proposed by Baumann and Rudin (16), and k_{cl} was represented as in the following equation:

$$k_{cl}=(dc_m/dt)/c_c(t)$$

In Baumann and Rudin's equation, Cc represented the cortical Gd-DTPA concentration and Cm represented the whole medullar GD-DTPA concentration. The slope of the TIC of the medullar (dc_m/dt) represented the uptake of Gd-DTPA in urine, while the cortical tracer concentration (c_c) closely resembled the vascular Gd-DTPA concentration. The time t was determined when there was the largest discrepancy between CO and M on DCE images; it ranged from 12 s to 18 s in the study and varied in each individual.

Histological Examination

All rats were sacrificed after the final MRI examination, and both kidneys were harvested for histopathological examination. The samples were fixed with 5% buffered formalin, embedded in paraffin, and then cut into 5 mm-thick sections. The sections were stained with hematoxylin and eosin (HE), and the microscopic changes of each sample were examined by an experienced pathologist who was blinded to the grouping. The alterations in renal tubules, including tubular dilation, epithelial cell vacuolization, desquamation and cast formation, as well as alterations of the interstitial tissue, including interstitial tissue edema and inflammatory cell infiltration were demonstrated. Renal damage was scored using a semi-quantitative method based on the injury area of involvement with a scale of 1 to 4 as follows: 1, absence of injury; 2, localized injury (<25% renal injury); 3, extended injury (<50% renal injury); and 4, severe injury (>50% renal injury) (21).

Statistical Analysis

The statistical analysis was performed with Statistical Product and Service Solutions (SPSS) software 12.0.1. Data were presented as mean ± SD for a normal distribution and median ± Q for a non-normal distribution. The Kolmogorov Smirnov test was applied to assess normally distributed data, and Levene's test was used for the variance homogeneity assay. Comparative analyses of SSI and k_{cl} values were performed via the least significant difference (LSD) at different time points. Kruskal-Wallis H test and Mann-Whitney U test were used for pathological damage score analyses. $P < 0.05$ was taken as a significant difference.

Results

Coronal T_2WI showed serial SI changes on the bilateral kidneys in four groups prior to (day 0) and after IRI (days 2, 5, 7 and 14) (Fig. 3). In healthy kidneys (day 0), CO and OSOM demonstrated similar moderate signal intensity and ISOM showed a relatively hyperintense signal. After the IRI procedure, the left OSOM in Group I and Group II began to appear as a hyperintense stripe (day 2) with distinct boundaries that radiated to the CO, and then broadened with obscure boundaries and were even brighter thereafter (day 5). Then, they began to shrink but still showed a hyperintense signal (day 7). Subsequently, the OSOM returned to normal size with residual bright strains. The hyperintense stripe of the OSOM in Group II was much brighter than that in Group I, which indicated more severe edema and worse injury in Group II. No notable changes could be observed in the left kidneys in Group III and Group IV and the right kidneys in all four groups at all time points.

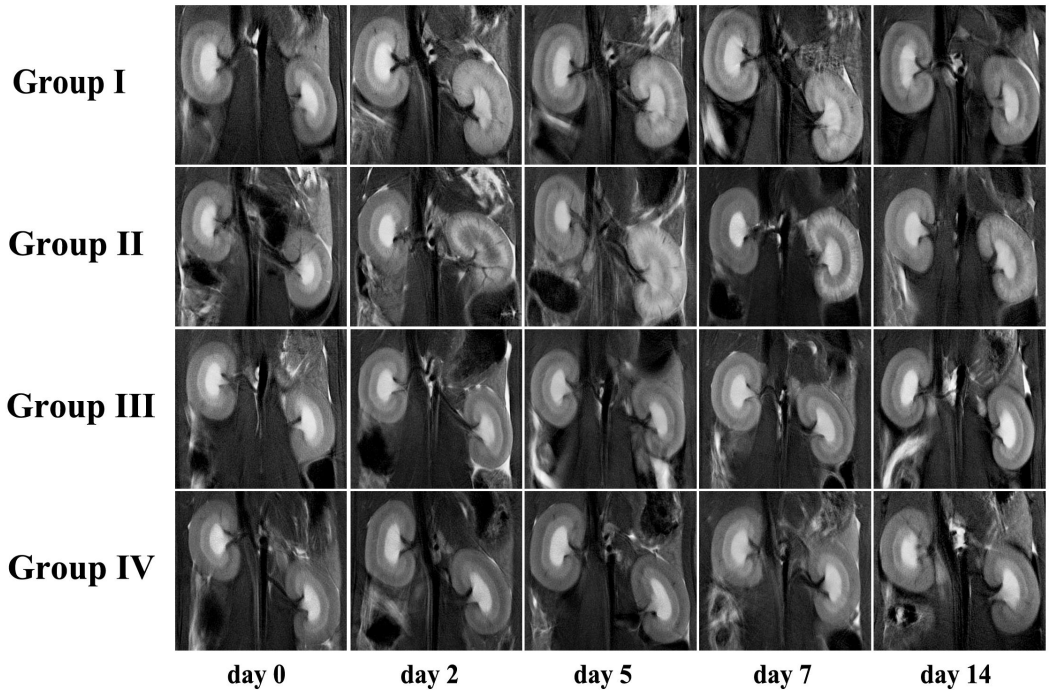

FIG. 3. Examples of fat-suppressed T_2WI images in the central coronal section of the bilateral kidneys prior to (day 0) and after IRI (days 2, 5, 7 and 14) in the four groups. The OSOM of the left kidneys began to appear as a hyperintense stripe on day 2 in Group I and Group II, with distinct boundaries that radiated to the renal cortex, and then broadened with obscure boundaries and were even brighter thereafter on day 5. Then, they began to shrink but still had a hyperintense signal on day 7. Subsequently, the OSOM returned to normal size with residual bright strains. The hyperintense stripe of the OSOM in Group II was much brighter than that in Group I. No notable changes were observed on the right kidneys in the four groups and the left kidneys in Group III and Group IV at all time points.

The average SSI of the bilateral OSOM in the four groups are listed in Table 1. SSI of bilateral OSOM on day 0 were not significantly different among the four groups. SSI of the left OSOM in Group I and Group II rose sharply on day 2, and they were higher than those of the other kidneys (the right kidneys in all four groups and the left kidneys in Group III and Group IV) at all time points after IRI, which fluctuated within quite a narrow range. SSI of the left OSOM in Group I on day 5 and

day 7 were lower than those in Group II ($P = 0.004$, $P < 0.001$, respectively). No significant differences in SSI existed between any two of the other kidneys (Fig. 4).

TABLE 1

Average SSI (mean ± SD) of the OSOM on bilateral kidneys prior to (day 0) and after IRI (days 2, 5, 7 and 14) among the four groups

Group	day 0		day 2		day 5		day 7		day 14	
	R	L	R	L	R	L	R	L	R	L
Group I	3.10± 0.32	3.10± 0.72	3.12± 0.29	4.89± 0.84	2.91± 0.46	4.10± 0.64	2.37± 0.34	4.78± 0.97	3.02± 0.63	4.36± 0.58
Group II	2.66± 0.35	2.89± 0.40	2.75± 0.48	5.35± 0.98	2.84± 0.28	4.95± 0.59	2.51± 0.51	6.40± 0.94	2.77± 0.41	4.98± 1.20
Group III	2.83± 0.45	2.81± 0.35	3.22± 0.50	3.23± 0.39	3.18± 0.41	3.23± 0.23	3.01± 0.53	3.08± 0.57	3.02± 0.43	3.05± 0.21
Group IV	3.00± 0.39	2.97± 0.33	2.99± 0.42	3.21± 0.40	3.18± 0.36	2.83± 0.29	2.92± 0.52	2.69± 0.42	3.02± 0.42	2.93± 0.54

R indicates the OSOM of the right kidney; L, the OSOM of the left kidney.

Group I, IRI+MitoQ; Group II, IRI+Saline;

Group III, Normal+MitoQ; Group IV, Normal+Saline.

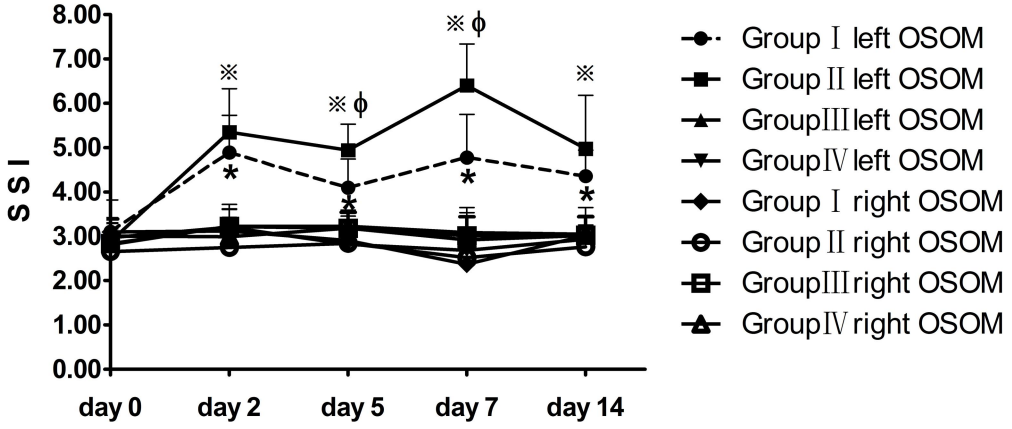

*FIG. 4. Graphs of SSI of the OSOM on bilateral kidneys in the four groups before (day 0) and after IRI (days 2, 5, 7 and 14). SSI of the bilateral OSOM on day 0 were not significantly different among the four groups. SSI of the left OSOM in Group I and Group II rose sharply on day 2, and they were higher than those of the other kidneys (the right kidneys in all the groups and the left kidneys in Group III and Group IV) at all time points after IRI, which fluctuated within a narrow range. SSI of the left OSOM in Group I on day 5 and day 7 were lower than those in Group II (P = 0.004, P < 0.001, respectively). No significant differences in SSI existed between any two of the other kidneys. Significant differences of SSI of the OSOM between the left kidneys in Group I and the other kidneys are indicated as * (P < 0.05); those between the left kidneys in Group II and the other kidneys are indicated as ※ (P < 0.05); those between the left kidneys in Group I and the left kidneys in Group II are indicated as φ (P < 0.05).*

DCE-MRI showed that the initial SI increase in the cortex was slower and lower in the left kidneys than in the right kidneys in Group I and Group II, and the thicknesses of the cortex were thinner as well; however, the bilateral kidneys in Group III and Group IV were enhanced to the same extent. The decrease in the left cortex enhancement was less obvious in Group I than in Group II. A clear corticomedullary boundary could be seen in all the groups until 18 s. The renal medulla of the right kidneys in the four groups began to enhance at 24 s, and then the

medulla achieved almost identical enhancement as the cortex during 48 s-60 s. However, there was a notable delay in the enhancement for the left kidneys in Group I and Group II (Fig. 5).

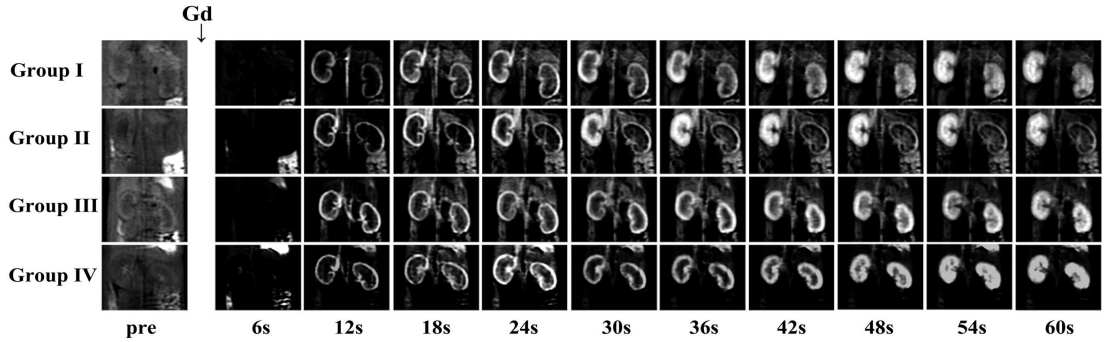

FIG. 5. Examples of the dynamic contrast-enhanced images of bilateral renal regions in four groups on day 2 after IRI. On precontrast images (pre), bilateral kidneys in four groups were seen with similar signal intensity (SI). After the administration of Gd-DTPA (Gd ↓), the initial SI increase in the cortex was slower and lower in the left kidneys than in the right kidneys in Group I and Group II, and the thicknesses of the cortex were thinner as well; however, the bilateral kidneys in Group III and Group IV were enhanced to the same extent. The decrease of the left cortex enhancement was less obvious in Group I than in Group II. A clear corticomedullary boundary could be seen in all the groups until 18 s. The renal medulla of the right kidneys in the four groups began to enhance at 24 s, after which the medulla achieved almost identical enchantment as the cortex during 48 s-60 s. However, there was a notable delay in the enhancement for the left kidneys in Group I and Group II.

K_{cl} values for the four groups at different time points are listed in Table 2. K_{cl} values of the bilateral kidneys in the four groups on day 0 were not significantly different. K_{cl} values of the left kidneys dropped dramatically on day 2 in Group I and Group II, after which the values in Group I began to rise gradually but were still below the normal level; meanwhile, the values in Group II continued to drop until day 5, and they reached a much lower level than in Group I. K_{cl} values of the left kidneys in Group I and Group II were lower than those of the other kidneys (the right kidneys in

all the groups and the left kidneys in Group III and Group IV) after IRI. K_{cl} values of the left kidneys in Group I were higher than those in Group II at all time points after IRI ($P = 0.002$, $P < 0.001$, $P = 0.001$, $P < 0.001$). No significant difference in k_{cl} values existed between any two of the other kidneys (Fig. 6).

TABLE 2

Average k_{cl} values (mean ± SD) of the bilateral kidneys prior to (day 0) and after IRI (days 2, 5, 7 and 14) among the four groups

Group	day 0		day 2		day 5		day 7		day 14	
	R	L	R	L	R	L	R	L	R	L
Group I	2.46± 0.10	2.38± 0.11	2.56± 0.28	1.64± 0.24	2.53± 0.25	1.92± 0.18	2.57± 0.18	2.07± 0.29	2.58± 0.09	2.19± 0.24
Group II	2.48± 0.17	2.43± 0.17	2.36± 0.12	1.29± 0.15	2.53± 0.08	1.22± 0.28	2.47± 0.08	1.60± 0.30	2.46± 0.10	1.64± 0.28
Group III	2.42± 0.18	2.40± 0.12	2.41± 09	2.43± 0.12	2.50± 0.13	2.52± 0.15	2.48± 0.13	2.51± 0.15	2.47± 0.11	2.49± 0.13
Group IV	2.38± 0.12	2.40± 0.07	2.50± 0.11	2.46± 0.09	2.51± 0.11	2.51± 0.18	2.59± 0.16	2.48± 0.16	2.54± 0.14	2.49± 0.12

R indicates the right kidney; L, the left kidney.

Group I, IRI+MitoQ; Group II, IRI+Saline;

Group III, Normal+MitoQ; Group IV, Normal+Saline.

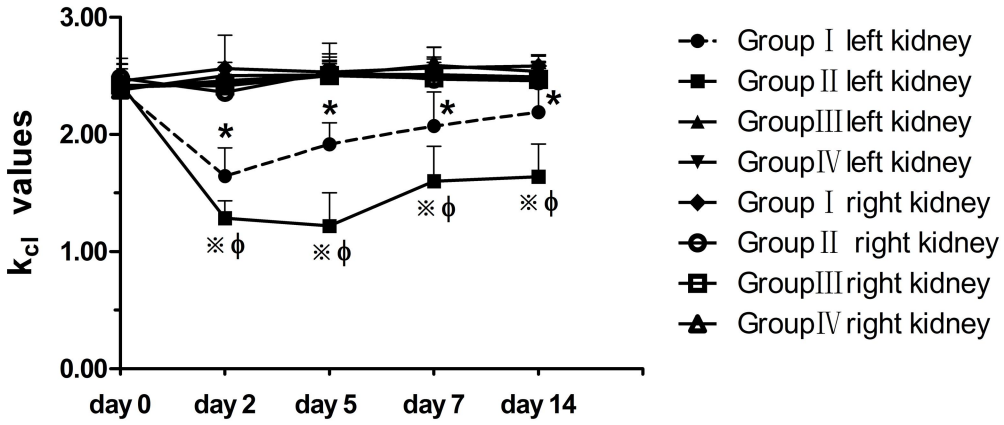

*FIG. 6. Graphs of the longitudinal changes of k_{cl} values on bilateral kidneys in the four groups before (day 0) and after IRI (days 2, 5, 7 and 14). K_{cl} values of the kidneys in all the groups on day 0 were at approximately the same level. K_{cl} values of the left kidneys dropped dramatically on day 2 in Group I and Group II, after which the values in Group I began to rise gradually but were still below the normal level; the values in Group II continued to drop until day 5, and they reached a much lower level than in Group I. K_{cl} values of the left kidneys in Group I and Group II were lower than those of the other kidneys (the right kidneys in all the groups and the left kidneys in Group III and Group IV) after IRI. K_{cl} values of the left kidneys in Group I were higher than those in Group II at all time points after IRI ($P = 0.002$, $P < 0.001$, $P = 0.001$, $P < 0.001$). No significant differences in k_{cl} values existed between any two of the other kidneys. Significant differences of k_{cl} values between the left kidneys in Group I and the other kidneys are indicated as * ($P < 0.05$); those between the left kidneys in Group II and the other kidneys are indicated as ※ ($P < 0.05$); those between the left kidneys in Group I and the left kidneys in Group II are indicated as φ ($P < 0.05$).*

The renal tissue analysis involved alterations in renal tubules (tubular dilation, epithelial cell vacuolization, desquamation and cast formation) and alterations in interstitial tissue (interstitial tissue edema and inflammatory cell infiltration), which

were the most obvious in the OSOM of the left kidneys in Group II, and such ischemic tubulointerstitial abnormalities were less predominant in the left kidneys in Group I; the other kidneys exhibited minimal pathological changes (Fig. 7). Only the left kidneys in Group I and Group II demonstrated significantly increased renal damage scores compared with the other kidneys ($P < 0.05$ and $P < 0.001$ respectively), and the median renal damage score of the left kidneys in Group II was significantly higher than that in Group I ($P < 0.001$) (Table 3).

TABLE 3

Pathological damage scores (median±Q) of the kidneys among the four groups

	Group I	Group II	Group III	Group IV
L	2.00±0.25$^{\varphi *}$	4.00±0.25$^{※}$	1.00±1.00	1.00±1.00
R	1.00±1.00	1.00±1.00	1.00±1.00	1.50±1.00

L indicates the left kidney; R, the right kidney.

Group I, IRI+MitoQ; Group II, IRI+Saline;

Group III, Normal+MitoQ; Group IV, Normal+Saline.

$^{\varphi}P < 0.05$ compared with the left kidneys in Group II . $^{*}P < 0.05$ compared with the other kidneys. ※ $P < 0.05$ compared with the other kidneys.

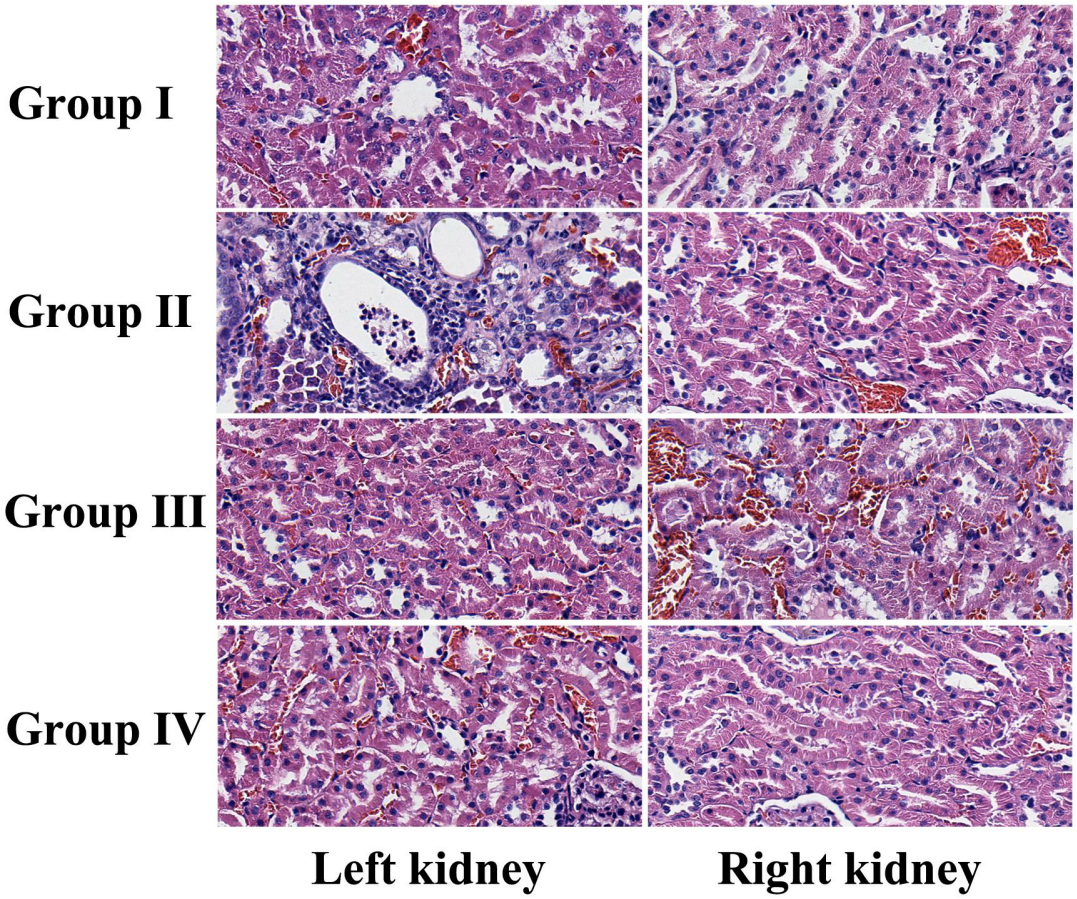

FIG. 7. Microscopic specimens with HE staining (× 400) of the bilateral kidneys on day 14 after IRI in the four groups. Tubular dilatation, tubular epithelial cell vacuolization, desquamation and cast formation, as well as interstitial tissue edema and inflammatory cell infiltration were observed in the left kidneys in Group II, and they were less predominant in the left kidneys in Group I. The most severe lesions were observed in renal tubules and interstitial tissue located in the OSOM. The pathological changes in other kidneys were minimal.

Discussion

In this study, we showed that the mitochondria-targeted antioxidant MitoQ could reduce the severity of renal damage caused by IRI using the longitudinal observation of T_2WI and DCE-MRI for the first time, which was confirmed by histopathological evaluation.

During renal IRI, the harmful hydrogen peroxide and ROS superoxide were critically increased from the mitochondria, causing damage to cellular lipids. Moreover, mitochondrial oxidative damage could destroy the ATP supply from mitochondria after reperfusion and lead to mitochondrial permeability transition pores and finally

cell death (9). Growing evidence has shown the OSOM is sensitive to hypoperfusion (14,22). And the major damage occurs on proximal convoluted tubules which are located on the OSOM: Ysebaert et al reported that up to 80% of proximal tubular cells in the OSOM were extensively damaged within 12 h after clamping the renal artery for 60 min followed by reperfusion in a rat model (23). The increased SI of the OSOM on T_2WI on IRI kidneys may be related to the increased tissue water content caused by tissue edema and reperfusion. The renal histopathological findings in the present study also confirmed that the most severe lesions after IRI were observed in renal tubules and interstitial tissue located in the OSOM.

MitoQ reaches its maximum at 5 min in the kidney tissue after iv injection (24), thus, in this study, the injection via the tail vein 15 min before the beginning of ischemia could enable MitoQ to be taken up completely. Furthermore, the half-life of MitoQ for the kidney is 4 h, and 80% of MitoQ could not be eliminated until 24 h after iv injection (24), which helps MitoQ work for several hours. The generation of lipid peroxyl radicals and enhanced ROS could be decreased within the mitochondria by MitoQ, preventing mitochondrial oxidative damage (11), which can explain the lower SSI and the higher k_{cl} values of IRI kidneys in the MitoQ pretreatment group than in the saline control group. However, MitoQ had little effect on healthy renal function (healthy kidneys with MitoQ pretreatment and saline control shared similar renal function parameters), which might be due to the normal balance between the cells' defense mechanism and the ROS production being maintained by the cellular redox homeostasis, while MitoQ worked only to lower the oxidative stress caused by the imbalance from the excessive production of ROS.

Noninvasive monitoring of the progression associated with renal IRI is of great importance (25). However, it is also a methodological challenge because all the currently available techniques have limitations. Many researchers have monitored renal function with biochemical assays, e.g., serum creatinine levels, which could detect only the overall renal function of both kidneys (9,26,27). To recognize and monitor unilateral renal function, these studies had to use a rodent model subjected to contralateral nephrectomy (28-31) or clamping of the bilateral renal arteries (32-36),

which established a different pathological environment from that found in clinical practice. Moreover, repeatedly taking blood samples for longitudinal studies might interfere with the physiologic environment in a small animal model. Dynamic scintigraphic renography is ideal for measuring unilateral GFR (37), however, the method cannot be performed on rodent kidneys because both the kidney and aorta are too small to be delineated.

Several mathematical models have been proposed to measure unilateral renal function from DCE-MRI. Among of them, the Baumann-Rudin model is unique because it does not depend on arterial input function (AIF), thus exempting the SI measurement error associated with motion and magnetic susceptible artifacts on the aorta or renal artery. This is a great advantage to be applied in rodent models since their diameters are very small. The normal level of k_{cl} value (2.44±0.14/min) in the present study differed from that of the literature published in the years 2000 and 2002, which ranged from 3.4±0.5/min (16) to 1.53±0.09/min (17). There may be several reasons for the discrepancy. First, the experiment in year 2002 was carried out on Wistar-Kyoto rats. Second, the previous images were obtained with much longer acquisition times (over 10 s) and had poor spatial resolution.

There were several limitations in our study. First, the sample size was small; a larger sample study should be carried out for further investigation. In this way, dose-dependent effects might be taken into consideration. Second, the renal systemic fibrosis induced by gadolinium was not taken into account. The current study aimed to evaluate MitoQ for its protective effect on renal function based on DCE-MRI in the research field instead of necessarily suggesting that clinical patients undergoing DCE-MRI in practice. It would be interesting to determine whether non-contrast functional MRI could play a role in the evaluation of renal IRI, and this is an issue we would like to investigate in the future.

In conclusion, T_2 signal intensities and k_{cl} values could demonstrate the presence of renal IRI and MitoQ could reduce the severity of renal damage in rodent IRI models.

REFERENCES

1. Smith ZL. Current Status of Minimally Invasive Surgery for Renal Cell Carcinoma. Curr Urol Rep 2016;17:43.
2. Schneider MJ, Dietrich O, Ingrisch M, Helck A, Winter KS, Reiser MF, Staehler M, Casuscelli J, Notohamiprodjo M. Intravoxel incoherent motion Magnetic Resonance Imaging in partially nephrectomized kidneys. Invest Radiol 2016;51:323-330.
3. Thompson RH, Lane BR, Lohse CM, Leibovich BC, Fergany A, Frank I, Gill IS, Blute ML, Campbell SC. Every minute counts when the renal hilum is clamped during partial nephrectomy. Eur Urol 2010;58:340-345.
4. Kaouk JH, Malkoç E. Is robotic partial nephrectomy convenient for solitary kidney ? Turk J Urol 2016;42:127-129.
5. Hu L, Chen J, Yang X, et al. Assessing Intrarenal Non-perfusion and Vascular Leakage in Acute Kidney Injury withzz ^{19}F MRI and Perfluorocarbon Nanoparticles. Magn Reson Med 2014;71:2186-2196.
6. Kalogeris T, Bao Y, Korthuis RJ. Mitochondrial reactive oxygen species: a double edged sword in ischemia/reperfusion vs preconditioning. Redox Biol 2014;2:702-714.
7. Guan W, Wang Z, Liu Y, Han Y, Ren H, Eric Wang W, Yang J, Zhou L, Zeng C. Protective effects of tirofiban on ischemia/reperfusion-induced renal injury in vivo and in vitro. Eur J Pharmacol 2015;761:144-152.
8. Eltzschig HK, Eckle T. Ischemia and reperfusion--from mechanism to translation. Nat Med 2011;17:1391-1401.
9. Dare AJ, Bolton EA, Pettigrew GJ, Bradley JA, Saeb-Parsy K, Murphy MP. Protection against renal ischemia-reperfusion injury in vivo by the mitochondria targeted antioxidant MitoQ. Redox Biol 2015;5:163-168.
10. Malek M, Nematbakhsh M. Renal ischemia/reperfusion injury; from pathophysiology to treatment. J Renal Inj Prev 2015;4:20-27.

11. Oyewole AO, Birch-Machin MA. Mitochondria-targeted antioxidants. FASEB J 2015;29:4766-4771.
12. Zöllner FG, Zimmer F, Klotz S, Hoeger S, Schad LR. Renal perfusion in acute kidney injury with DCE-MRI: deconvolution analysis versus two-compartment filtration model. Magn Reson Imaging 2014;32:781-785.
13. Hueper K, Rong S, Gutberlet M, et al. T2 relaxation time and apparent diffusion coefficient for noninvasive assessment of renal pathology after acute kidney injury in mice: comparison with histopathology. Invest Radiol 2013;48:834-842.
14. Munshi R, Hsu C, Himmelfarb J. Advances in understanding ischemic acute kidney injury. BMC Med 2011;9:11.
15. Taylor J, Summers PE, Keevil SF, Saks AM, Diskin J, Hilton PJ, Ayers AB. Magnetic resonance renography: optimisation of pulse sequence parameters and Gd-DTPA dose, and comparison with radionuclide renography. Magn Reson Imaging 1977;15:637-649.
16. Baumann D, Rudin M. Quantitative assessment of rat kidney function by measuring the clearance of the contrast agent Gd (DOTA) using dynamic MRI. Magn Reson Imaging 2000;18:587–595.
17. Laurent D, Poirier K, Wasvary J, Rudin M. Effect of essential hypertension on kidney function as measured in rat by dynamic MRI. Magn Reson Med 2002;47:127-134.
18. Mendichovszky I, Pedersen M, Frøkiær J, Dissing T, Grenier N, Anderson P, McHugh K, Yang Q, and Gordon I. How accurate is dynamic contrast-enhanced MRI in the assessment of renal glomerular filtration rate? A critical appraisal. J Magn Reson Imaging 2008;27:925–931.
19. Grenier N, Mendichovszky I, de Senneville B. D, Roujol S, Desbarats P, Pedersen M, Wells K, Frokiaer J, Gordon I. Measurement of glomerular filtration rate with magnetic resonance imaging: principles, limitations, and expectations. Semin Nucl Med 2008;38:47–55.
20. Shahbazi-Gahrouei D, Williams M, Allen BJ. In vitro study of relationship

between signal intensity and gadolinium-DTPA concentration at high magnetic field strength. Australas Radiol 2001;45:298-304.

21. Alexandropoulos D, Bazigos GV, Doulamis IP, et al. Protective effects of N-acetylcystein and atorvastatin against renal and hepatic injury in a rat model of intestinal ischemia-reperfusion. Biomed Pharmacother 2017;89:673-680.
22. Haase VH. Mechanisms of hypoxia responses in renal tissue. J Am Soc Nephrol 2013;24:537-541.
23. Ysebaert DK, De Greef KE, Vercauteren SR, Ghielli M, Verpooten GA, Eyskens EJ, De Broe ME. Identification and kinetics of leukocytes after severe ischaemia/reperfusion renal injury. Nephrol Dial Transplant 2000;15:1562-1574.
24. Porteous CM, Logan A, Evans C, Ledgerwood EC, Menon DK, Aigbirhio F, Smith RA, Murphy MP. Rapid uptake of lipophilic triphenylphosphonium cations by mitochondria in vivo following intravenous injection: Implications for mitochondria-specific therapies and probes. Biochim Biophys Act 2010;1800:1009-1017.
25. Nielsen PM, Szocska Hansen ES, Nørlinger TS, Nørregaard R, Bonde Bertelsen L, Stødkilde Jørgensen H, Laustsen C. Renal ischemia and reperfusion assessment with three-dimensional hyperpolarized 13 C,15 N2-urea. Magn Reson Med 2016;76:1524-1530.
26. Zhang JL, Rusinek H, Chandarana H, Lee VS. Functional MRI of the kidneys. J Magn Reson Imaging 2013;37:282-293.
27. Sari-Sarraf F, Pomposiello S, Laurent D. Acute impairment of rat renal function by L-NAME as measured using dynamic MRI. MAGMA 2008;21:291-297.
28. Turrens JF, Beconi M, Barilla J, Chavez UB, McCord JM. Mitochondrial generation of oxygen radicals during reoxygenation of ischemic tissues. Free Radic Res Commun 1991;12–13:681–689.
29. Prókai A, Fekete A, Bánki NF, et al. Renoprotective effect of erythropoietin in rats subjected to ischemia/reperfusion injury: gender differences. Surgery 2011;150:39-47.
30. Ishii Y, Sawada T, Murakami T, Sakuraoka Y, Shiraki T, Shimizu A, Kubota

K, Fuchinoue S, Teraoka S. Renoprotective effect of erythropoietin against ischaemia-reperfusion injury in a non-human primate model. Nephrol Dial Transplant 2011;26:1157-1162.

31. Zhang J, Zou YR, Zhong X, Deng HD, Pu L, Peng K, Wang L. Erythropoietin pretreatment ameliorates renal ischaemia-reperfusion injury by activating PI3K/Akt signalling. Nephrology (Carlton) 2015;20:266-272.
32. Hu L, Yang C, Zhao T, Xu M, Tang Q, Yang B, Rong R, Zhu T. Erythropoietin ameliorates renal ischemia and reperfusion injury via inhibiting tubulointerstitial inflammation. J Surg Res 2012;176:260-266.
33. Patel NS, Kerr-Peterson HL, Brines M, et al. Delayed administration of pyroglutamate helix B surface peptide (pHBSP), a novel nonerythropoietic analog of erythropoietin, attenuates acute kidney injury. Mol Med 2012;18:719-727.
34. Ardalan MR, Estakhri R, Hajipour B, et al. Erythropoietin ameliorates oxidative stress and tissue injury following renal ischemia/reperfusion in rat kidney and lung. Med Princ Pract 2013;22:70-74.
35. Imamura R, Moriyama T, Isaka Y, Namba Y, Ichimaru N, Takahara S, Okuyama A. Erythropoietin protects the kidneys against ischemia reperfusion injury by activating hypoxia inducible factor-1alpha. Transplantation 2007;83:1371-1379.
36. Patel NS, Sharples EJ, Cuzzocrea S, Chatterjee PK, Britti D, Yaqoob MM, Thiemermann C. Pretreatment with EPO reduces the injury and dysfunction caused by ischemia/reperfusion in the mouse kidney in vivo. Kidney Int 2004;66:983-989.
37. Chen B, Zhang Y, Song X, Wang X, Zhang J, Fang J. Quantitative estimation of renal function with dynamic contrast-enhanced MRI using a modified two-compartment model. PLoS One 2014;9:e105087.